CHEMISTRY OF MATERIALS

ARTICLE

pubs.acs.org/cm

Biomimetic Silicification of Fibrous Chitin from Diatoms

Katrin Spinde,[†] Martin Kammer,[†] Katja Freyer,[†] Hermann Ehrlich,[†] John N. Vournakis,[‡] and Eike Brunner*[,†]

[†]Technische Universität Dresden, Fachrichtung Chemie und Lebensmittelchemie, Bioanalytische Chemie, 01062 Dresden, Germany

[‡]Marine Polymer Technologies, Inc., Burlington, Massachusetts 01803, United States

ABSTRACT: Poly-*N*-acetyl-D-glucosamine (*p*-GlcNAc, chitin) is a biopolymer found in various organisms and in forms such as sheets, membranes, and fibers. Its presence in numerous calcium-based biominerals is well-known. Recently, chitin was even found in silica-based biominerals. While it is well-established that various proteins and even long-chain polyamines are involved in silica biomineralization events, the role of polysaccharides is rather poorly understood. Furthermore, silica-chitin nanocomposites and silica-coated chitin constructs are increasingly important, e.g., in materials science and for biomedical applications. Therefore, we have investigated the interaction between *p*-GlcNAc in fibers and silicic acid/silica species *in vitro*, using ^{13}C and ^{29}Si NMR as well as Raman spectroscopy, in combination with microscopic techniques. Furthermore, the kinetics of silica condensation in the presence/absence of *p*-GlcNAc fibers could be analyzed using the molybdenum blue test.

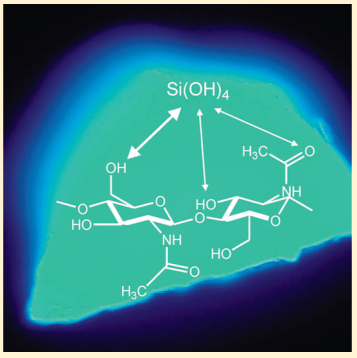

KEYWORDS: ^{13}C and ^{29}Si NMR, hybrid materials, nanocomposites, silica, poly-N-acetyl-D-glucosamine, molybdenum blue test

INTRODUCTION

During the past years, different biomolecules were found to be involved in silica biomineralization events. Examples are strongly post-translationally modified proteins, so-called silaffins[1−3] in diatoms as well as silicateins in sponges.[4,5] Long-chain polyamines are also involved in biosilica formation.[6] Furthermore, the highly acidic silacidins were recently discovered in diatom biosilica.[7]

Apart from the aforementioned biomolecules, polysaccharides such as chitin and others are also sometimes embedded in biominerals.[8−10] Chitin—the second-most-abundant polysaccharide on Earth after cellulose—is a structural biopolymer found in numerous animals. It consists of β-1,4-glycan-linked *N*-acetyl-D-glucosamine (GlcNAc) units.[11,12] It occurs in the exoskeletons of crabs, lobsters, insects, and several other organisms, as well as in the cell walls of fungi and numerous calcium-based biominerals.[13] During the past years, its presence in several demosponges from the Verongida family was discovered.[14−16] Chitin could even be found to be embedded in sponge biosilica.[17] Many diatoms, such as *Thalassiosira* sp., produce external fibers which consist of highly crystalline β-chitin.[18] Furthermore, the siliceous cell walls of the diatom *Thalassiosira pseudonana*[8] exhibit internal chitin-based networks. This internal chitin is rather amorphous and contains a high amount of other bimolecules, such as proteins.

Silica-organic hybrid materials,[19] such as silica-chitin hybrids, also gain interest, with respect to biomimetic synthesis approaches. Chitin from cuttlebone of *Sepia officinalis* was previously used for the synthesis of biomimetic silica-organic hybrid materials, because of its controllable size, shape, organization, and porosity.[20] Furthermore, silica-chitin hybrid materials are recently under investigation for biomedical applications, such as wound dressing and as scaffolds in tissue engineering, because of their favorable wound healing, antibacterial, and anti-inflammatory properties.[11,21−23] Demadis et al. showed that zwitterionic phosphomethylated chitosan partly inhibits the polycondensation of silicic acid.[24] Chitosan can be obtained from chitin by deacetylation. A chitin-based compound is denoted as chitosan if the degree of deacetylation exceeds 50%. Recently, Alonso and Belamie[25] published a novel colloid-based approach for large-scale synthesis of silica-chitin nanocomposites of controlled texture and morphology. In contrast to the present work, Alonso and Belamie[25] used surface-deacetylated chitin in order to facilitate silica deposition. Furthermore, tetraethyl orthosilicate (TEOS) served as the silica precursor compound in this previous study.[25]

However, our knowledge about the role of chitin in silica biomineralization processes, as well as its interactions with silicic acid/silica species, is very limited. The aim of the present work is to better understand these interactions at a molecular level, using the external fibrous chitin extracted from diatoms (see below) and the biologically relevant silica precursor compound, namely, orthosilicic acid.[26−28] For this purpose, β-chitin extracted from diatoms following a patented recipe[29,30] was silicified *in vitro* using orthosilicic acid solutions at pH 5.5. This pH value is approximately found in the silica deposition vesicle during diatom cell wall biosynthesis.[31] β-chitin is used in our experiments, because of its ability to swell. This should facilitate the interaction with silicic acid species in solution. Silicification of the β-chitin is demonstrated, verified, and characterized at a molecular level via the combined use of liquid and solid-state NMR, Raman spectroscopy, and microscopy, as well as the established molybdenum blue test.[32]

Received: March 7, 2011
Revised: April 15, 2011
Published: May 06, 2011

MATERIALS AND METHODS

Materials. Within the present work, *p*-GlcNAc was extracted from diatoms following the published method.[29,30] The method relies primarily on the ability to dissolve the diatom exoskeleton using hydrogen fluoride treatment with minimal damage to the *p*-GlcNAc fibers. The fibrous chitin extracted from diatoms in the described manner is mainly β-chitin, as could also be confirmed by ^{13}C MAS NMR spectroscopy. However, the extraction procedure may result in the transformation of minor amounts of the metastable β-chitin to α-chitin or simply disordered *p*-GlcNAc, as indicated by the presence of a subset of small ^{13}C NMR signals, apart from the well-known narrow and intense signals characteristic for β-chitin.[14,33] Therefore, the fibrous chitin used in our experiments is denoted as *p*-GlcNAc throughout the present paper. The polyallylamine hydrochloride (PAH, Aldrich, Germany) molecule exhibits a repeated unit of the structure $[-CH_2CH(CH_2NH_2)\cdot HCl-]_n$ with $n \approx 160$ corresponding to a molecular weight of 15 000 g/mol. All samples were prepared using purified distilled water (filter system: Elga—Purelab Classic, Germany; filter: Gelman Sciences (Supor DCF), 0.2 μm). In the following, this will be denoted as ultrapure water.

Sample Preparation for Microscopy/SEM, Raman and NMR Spectroscopy. Three milligrams of *p*-GlcNAc (short fibers) were suspended in 5 mL of a 100-mM sodium metasilicate (Sigma—Aldrich, Germany) solution (pH ~12.8) and titrated with hydrochloric acid (2.4 M) to the desired pH of 5.5 ± 0.1. That means the starting volume increased by 8.6% during this procedure. For a better dispersion of *p*-GlcNAc in silicic acid, the sample was stirred until a gel was formed. After 24 h, the gel was centrifuged (9000 U/min, room temperature, 15 min) and dried overnight at 318 K.

Sample Preparation for Kinetic Analysis. A 100-mM solution of SiO_2 was prepared by dissolving 284.2 mg sodium metasilicate-nonahydrate in 10 mL of ultrapure water. Six milligrams of *p*-GlcNAc were added to the stock solution (Si:O/N = 5:1). The solution (pH ~12.8) was titrated to the desired pH of 5.5 ± 0.1 via the addition of hydrochloric acid (2.4 M) under continuous stirring. The solution was split equally into 10 aliquots, transferred into Eppendorf vials, and set aside without stirring. The *p*-GlcNAc/silicic acid solution was analyzed by the molybdenum blue test every 30 min for the first 2 h and at 4, 6, 8, 24 h after titration.

For the molybdenum blue test, the following solutions were prepared: (a) 3.1 g ammonium molybdate tetrahydrate (Sigma—Aldrich, Germany) dissolved in 50 mL of 1.0 M sulfuric acid; (b) 6.3 g of oxalic acid dehydrates (Sigma—Aldrich, Germany), and (c) 1.76 g of ascorbic acid, each dissolved in 50 mL of ultrapure water.

Each sample was centrifuged (9000 U/min, room temperature, 5 min) and a specific volume, different from sample to sample, was diluted to 100 mL in a volumetric plastic flask. Seventy five microliters (75 μL) of ammonium molybdate solution were added to 1.5 mL of the diluted solution, mixed well, and left undisturbed for 10 min. Afterward, 75 μL of oxalic acid were admixed. After a second waiting period of 1 min, 75 μL of the reducing agent ascorbic acid were added and the solution was equilibrated for further 10 min before the monosilicic acid concentration was determined photometrically (using a UV—VIS spectrophotometer (Varian Cary 50)) at a wavelength of 810 nm.

Scanning Electron Microscopy. Scanning electron microscopy (SEM) images were taken on a Zeiss Model DSM 982 Gemini system, using an accelerating voltage of 1.0 kV.

Fluorescence Microscopy. Light microscopy and fluorescence microscopy images of pure silica and silica—*p*-GlcNAc nanocomposite samples were taken on a Keyence Model BZ-8000 microscope at 10× magnification and an exposure time of 1/100 s for light microscopy images and 1 s for fluorescence microscopy images.

NMR Spectroscopy. Solid-state (CP) MAS NMR experiments were performed on a Bruker Avance 300 spectrometer, using a commercial double-resonance 4-mm MAS NMR probe operating at 75.47 MHz for ^{13}C and 59.63 MHz for ^{29}Si. Ramped ^{1}H—^{13}C cross-polarization (CP)[34,35] was used (contact time = 4 ms, repetition time = 2 s for ^{13}C and 20 s for ^{29}Si). SPINAL64 ^{1}H-decoupling[36] was applied during signal acquisition. The temperature of 293 K inside the rotor was calibrated using the ^{207}Pb chemical shift of lead nitrate as a temperature reference.[37] The chemical shifts were referenced relative to TMS. Liquid-state ^{29}Si NMR experiments were performed on the same spectrometer operating at 59.63 MHz for ^{29}Si, using a glass tube 10 mm in diameter (repetition time = 60 s). WALTZ16 ^{1}H-decoupling was applied during signal acquisition. The ^{29}Si isotope enriched samples were prepared from 96.7% ^{29}Si-labeled sodium metasilicate. The latter compound was synthesized from isotope-enriched $^{29}SiO_2$ (CortecNet), according to the established recipe.[38]

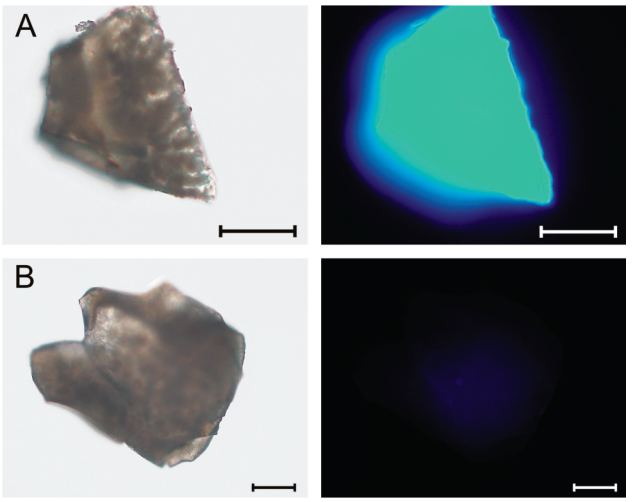

Figure 1. Light microscopic (left) and fluorescence microscopic (right) images of (A) silica-*p*-GlcNAc nanocomposite and (B) pure silica. Scale bar = 100 μm.

Raman Spectroscopy. Raman spectra were recorded on a Kaiser HoloLab Series 5000 microscope coupled to a *f*/1.8 Holospec spectrograph (Kaiser Optical Systems, Ann Arbor, MI) with a liquid-nitrogen-cooled CCD camera (Roper Scientific, Trenton, NH). A Toptica XTRA laser (Toptica Photonics AG, Gräfelfing, Germany) with an excitation wavelength of 785 nm was used, the spectral resolution was 4 cm^{-1}. All spectra were background-corrected.

RESULTS AND DISCUSSION

Figure 1 shows the light microscopic and fluorescence microscopic images of characteristic particles from the silica-*p*-GlcNAc nanocomposite (Figure 1A) as well as the control sample (Figure 1B). As can be seen, the *p*-GlcNAc-containing particle exhibits a characteristic fluorescence in the blue channel, which is typical for chitin. Since this fluorescence is homogeneously distributed over the entire particle, it can be concluded that the *p*-GlcNAc fibrils are indeed embedded into the sample (i.e., silicified) and homogenously distributed. Figure 2 shows scanning electron microscopy (SEM) images of the *p*-GlcNAc and pure silica reference samples, as well as the silicified *p*-GlcNAc. The pure *p*-GlcNAc (Figure 2A) consists of short, disordered fibers ca. 1.5—3 μm in length and 50—80 nm in average diameter. The pure silica sample (Figure 2B) shows unstructured plain silica blocks. If the silica is formed in the presence of *p*-GlcNAc, the sample exhibits some fibrous structures coated with silica (see Figures 2C and 2D). Since β-chitin is capable of swelling,[39] silica

dx.doi.org/10.1021/cm200677d |*Chem. Mater.* 2011, 23, 2973–2978

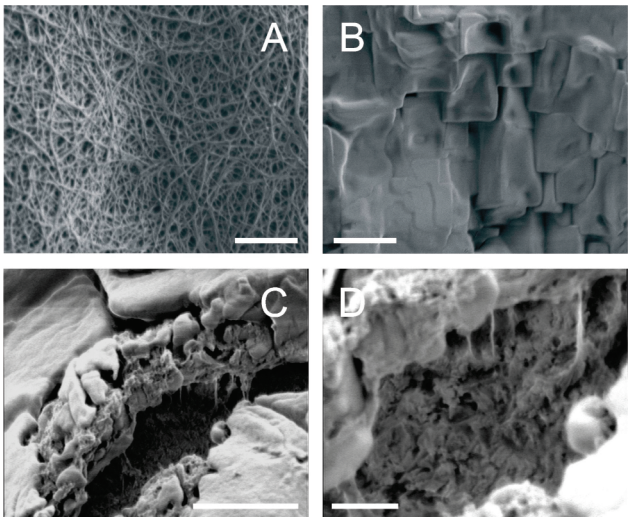

Figure 2. SEM images of (A) pure *p*-GlcNAc (scale bar = 2 μm); (B) pure silica (scale bar = 2 μm); and (C, D) silica-*p*-GlcNAc nanocomposite, showing the organization of the sample (scale bars are 2 μm in panel C and 500 nm in panel D).

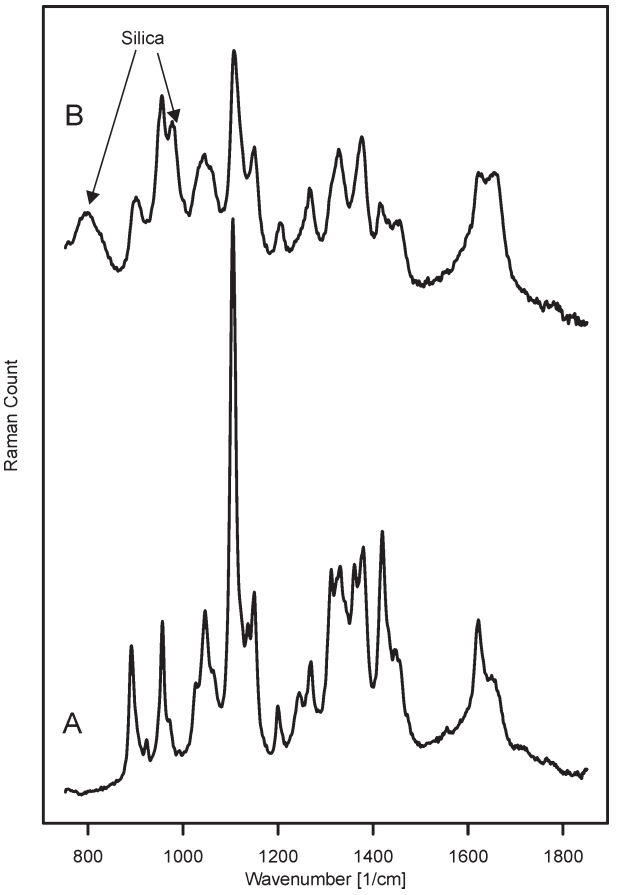

Figure 3. Background-corrected Raman spectra of (A) the reference *p*-GlcNAc fibers and (B) the *p*-GlcNAc fibers after silicification.

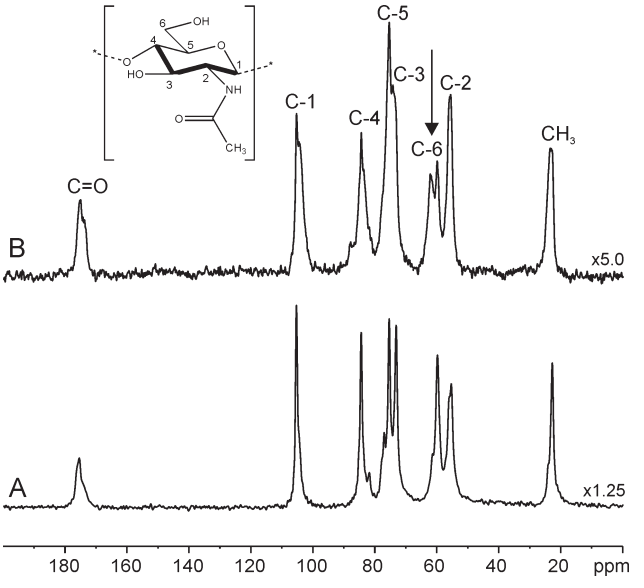

Figure 4. ^{13}C {^{1}H} CP MAS NMR spectra of pure *p*-GlcNAc (spectrum A) and silica−*p*-GlcNAc nanocomposite (spectrum B).

species are likely to penetrate into the *p*-GlcNAc fibers (see Figures 2C and 2D). This observation, in addition to the fluorescence microscopic observations (see Figure 1), indicates that the individual *p*-GlcNAc fibers are surface-coated with silica. In any case, the images shown in Figure 1 and 2 show that the silicification of *p*-GlcNAc, using sodium metasilicate, is successfully accomplished and results in a silica-*p*-GlcNAc nanocomposite material.

The incorporation of *p*-GlcNAc fibers into the silica should be accompanied by the formation of an interface with intermolecular interactions between the organic and inorganic phase. In order to detect such possible interactions, solid-state ^{13}C NMR and Raman spectroscopic investigations were performed. The Raman spectrum of silicified *p*-GlcNAc (Figure 3B) shows broadened and merged bands due to the silification, while the new band at 800 cm^{-1} is assigned to the deformation and network vibrations of silica. Less-intense bands become unobservable and the intensity of the band at 971 cm^{-1} increases because of an overlapping silica band in this region, while the spectrum remains similar to the reference short fibers (see Figure 3A). The spectrum of silicified *p*-GlcNAc is a mixture of signals due to silica and *p*-GlcNAc. Figure 4 shows the ^{13}C CP MAS NMR spectra of *p*-GlcNAc fibers (Figure 4A) and the silica−*p*-GlcNAc nanocomposite (Figure 4B). The ^{13}C CP MAS NMR spectrum of the pure *p*-GlcNAc fibers exhibits characteristic narrow and intense signals, because of the different carbon positions of β-chitin, as well as a minor subset of other signals at slightly different positions.[33,40−42] Silicification of *p*-GlcNAc obviously results in characteristic changes of the spectrum (see Figure 4B).

All signals exhibit signal broadening or even signal splitting. The most-pronounced effect is observed for carbon position C-6 (see Figure 5). The corresponding signal splits into two well-resolved signals in the silica−*p*-GlcNAc nanocomposite. One of these two signals (C-6(I)) occurs at 59.9 ppm, i.e., at exactly the same chemical shift as that observed for pure *p*-GlcNAc. This signal obviously represents unperturbed *p*-GlcNAc molecules. The other signal (C-6(II)) is shifted by 2.2 ppm and occurs at 62.1 ppm. Note that the chemical shift of C-6 in α-chitin amounts to ca. 61 ppm. The chemical shift of C-6(II) in the silica−*p*-GlcNAc nanocomposite is ca. 1 ppm higher. This indicates that the observed signal splitting of C-6 in the silica−*p*-GlcNAc

dx.doi.org/10.1021/cm200677d |*Chem. Mater.* 2011, 23, 2973–2978

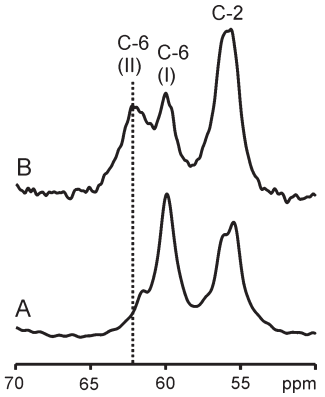

Figure 5. C-6 signals of the ^{13}C $\{^1H\}$ CP MAS NMR spectra of pure *p*-GlcNAc (spectrum A) and silica−*p*-GlcNAc nanocomposite (spectrum B).

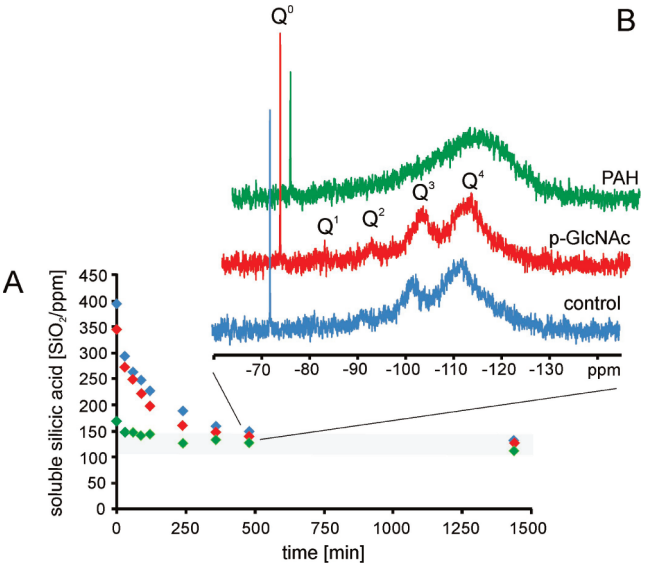

Figure 6. (A) Kinetics of the concentration of monosilicic acid and disilicic acid at pH 5.50 ± 0.1 in pure silicic acid solution (blue, control sample; red, a *p*-GlcNAc-containing solution; and green, a PAH-containing solution). The starting Si concentration at time "0 min" corresponds to the silicic acid concentration after titration to pH 5.50 ± 0.1. Note that the concentrations of silicic acid and organic additive were chosen such that the Si:O ratio in the *p*-GlcNAc-containing sample was equal to a Si:N ratio in the PAH-containing sample of ∼5:1. (B) The corresponding ^{29}Si HR NMR spectra after a condensation time of 480 min (color coding is the same as that given for panel A).

nanocomposites cannot simply be due to a partial transformation of β-chitin into α-chitin during our sample preparation. This conclusion is further corroborated by an inspection of our sample preparation procedure: The structural transformation of β-chitin to α-chitin happens under basic conditions after a treatment with 10 M sodium hydroxide (pK_a = 14) during treatment times of 1 h.[43] In contrast, our sample preparation only includes a very short exposure time (ca. 5 min) of the samples to pH 12.8 in 0.1 M sodium metasilicate solution (pK_a = 9) at room temperature, which means that our sample preparation occurs under considerably "milder" conditions. Therefore, the observed changes of the ^{13}C CP MAS NMR spectra—in particular, the characteristic splitting of the C-6 signal of *p*-GlcNAc—obviously indicate the interaction at the interface, in particular, between the OH groups and the silica species. Both signal components, C-6(I) and C-6(II) exhibit comparable intensities. Although quantitative information derived from CP spectra may exhibit considerable errors, we can nevertheless conclude that a significant fraction of the *p*-GlcNAc molecules (ca. 50%) are in contact with silica. The formation of a covalent Si−O−C bond seems to be unlikely, since one would expect a larger chemical shift change. Effects of this magnitude are, for example, found in hydrogen-bonded silica−poly(vinyl pyrrolidone) composites.[44] This observation means that hydrogen bond formation should result in carbon chemical shift changes of the observed order of magnitude. Therefore, the observed signal splitting of C-6 is most likely due to hydrogen bonding between the OH group located at C-6 and silicic acid oligomers/silica species. Interestingly, model studies, as well as observations recently made on sponge biosilica, indicate that hydrogen bonding between OH groups located at organic phases and silicic acid/silica species may play a role in silica biomineralization events.[45,46] Note that the C═O group in the silica−*p*-GlcNAc nanocomposite exhibits a pronounced shoulder (see Figure 4B). The chemical-shift difference between the original signal and this shoulder is of the order of 1 ppm.

Less-pronounced signal splitting is also observed for C-1. Furthermore, the peak height of the signal due to C-3, which also bears an OH group, decreases strongly, indicating severe line broadening. The other signals are more or less broadened and/or shifted, indicating that the interaction between the *p*-GlcNAc molecules and silica species results in a rearrangement of the entire *p*-GlcNAc molecule. The fact that a significant fraction of the *p*-GlcNAc molecules is influenced by silica formation shows that the fibers obviously swell and silica species penetrate into the interior.

The interactions between the OH groups located at *p*-GlcNAc—especially C-6-OH—and silica species could be demonstrated by our NMR studies. Therefore, a question arises: Do these interactions influence the kinetics of silicic acid condensation? Therefore, we studied the condensation of monosilicic acid and disilicic acid into higher oligomers via the molybdenum blue test, in combination with ^{29}Si HR NMR. The molybdenum blue test is capable of detecting the sum of the concentrations of monosilicic acid and disilicic acid.[47] Figure 6A shows the results of the molybdenum blue test. It turns out that *p*-GlcNAc (red) does not significantly influence the concentrations of monosilicic acid and disilicic acid within the considered time interval. After 270 min, the pure silicic acid solution, as well as the *p*-GlcNAc-containing sample, reach the equilibrium concentration determined by the solubility of silicic acid (2 mM = 120 ppm at pH 5.5).[47]

Obviously, the uncharged *p*-GlcNAc does not accelerate the initial steps of silicic acid condensation, although the molecules exhibit OH groups as interaction sites for silica species (see above). For comparison, we prepared another sample containing the highly charged polyallylamine hydrochloride (PAH, green) instead of *p*-GlcNAc. This model polyamine is well-characterized and is widely used in biomimetic silica synthesis experiments.[48−50] At pH 5.5, the positively charged PAH significantly accelerates the condensation of monosilicic acid and disilicic acid into higher oligomers (see Figure 6A).

The aforementioned equilibrium concentration is reached almost instantaneously after titration, and the samples exhibit a white precipitate. Obviously, this acceleration is due to the electrostatic interactions between the positively charged amine

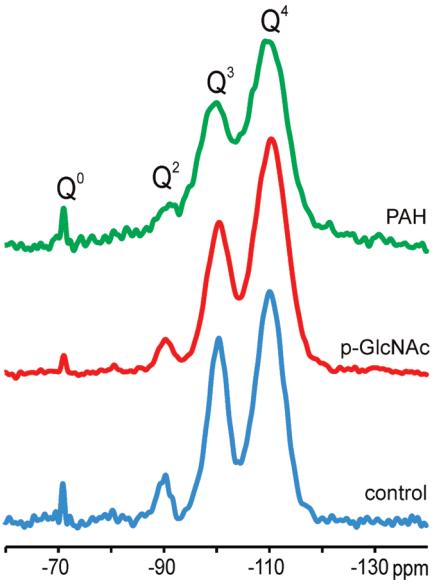

Figure 7. ^{29}Si MAS NMR spectra of control (blue trace), in the presence of *p*-GlcNAc (red trace), and PAH (green trace) after a condensation time of 24 h and a measurement time of 22 h.

functionalities of PAH and the negatively charged silicic acid/silica species in solution. This is confirmed by ^{29}Si HR NMR spectroscopy. ^{29}Si NMR is capable of detecting all Q^n-groups (where Q^n represents $Si(OSi)_n(OH)_{4-n}$). Time-resolved measurements of the (Q^0 + Q^1) group concentrations (data not shown) revealed the same behavior as that observed with the conventional molybdenum blue test (see Figure 6A). However, the spectra (Figure 6B) show another interesting difference between the *p*-GlcNAc- and PAH-containing samples: The spectrum of the *p*-GlcNAc-containing sample agrees almost perfectly with that of the pure silicic acid solution, even after 480 min, and exhibits broadened but well-resolved signals due to Q^2, Q^3, and Q^4. This means that *p*-GlcNAc does not significantly influence silicic acid polycondensation, even after 480 min. In contrast, the PAH-containing sample only exhibits a strongly broadened signal representing the sum of the Q^2, Q^3, and Q^4 group signals without any spectral resolution. Silicic acid oligomers are obviously immobilized by their attractive electrostatic interactions with the large and positively charged PAH molecules. In contrast, the weak hydrogen bonds between *p*-GlcNAc and silicic acid oligomers do not result in such an immobilization, even after 480 min. These observations clearly demonstrate the importance of electrostatic interactions for the speed of silica polycondensation. Alonso and Belamie[25] used surface-deacetylated chitin in their experiments. Surface deacetylation results in the transformation of a surface layer to chitosan with amine moieties (NH_2), which are charged in solution. These groups will—in analogy to our observations made for PAH with its NH_2 groups—enhance the speed of silica deposition at the surface.

However, since the ^{29}Si NMR signals are strongly broadened, especially for the PAH-containing sample, the degree of silica polycondensation, as reflected by the Q^4:Q^3:Q^2 ratio, cannot be measured in this ^{29}Si HR NMR measurement. In order to determine the influence of *p*-GlcNAc and PAH upon the Q^4:Q^3:Q^2 ratio obtained after longer time periods, we, therefore, have also carried out solid-state ^{29}Si NMR experiments on samples after a reaction time of 24 h. Since the measurement time required to detect spectra of sufficient signal-to-noise ratio was 22 h, the spectra shown in Figure 7 are representative for silica after 33 h (ca. 2000 min) of reaction time. Obviously, the control has a lower degree of silica condensation than the samples containing *p*-GlcNAc and PAH (see Table 1).

Table 1. Si−O−Si Angle (α),[a] FWHM ($\Delta\nu_{1/2}$), and Relative Signal Intensities of the ^{29}Si MAS NMR Signals

	Control			p-GlcNAc			PAH		
sample	Q^2	Q^3	Q^4	Q^2	Q^3	Q^4	Q^2	Q^3	Q^4
α [deg]	112	130	146	112	130	147	113	128	146
$\Delta\nu_{1/2}$ [ppm]	3.1	4.9	6.5	3.6	5.7	7.3	4.8	8.4	8.8
$\Delta\alpha_{1/2}$ [deg]	5	8	11	6	10	13	8	15	15
intensity ratio	0.1	0.7	1.0	0.1	0.5	1.0	0.1	0.5	1.0

[a] The distribution width ($\Delta\alpha_{1/2}$) of the Si−O−Si angle resulting from the measured FWHM also is given. The Q^2:Q^3:Q^4 intensity ratio of the ^{29}Si MAS NMR spectra is calculated using the program dmfit (current version: dmfit#20100301).[51]

After the long reaction time, however, *p*-GlcNAc results in a similar degree of silica condensation as PAH: (Q^2:Q^3:Q^4) ratios of (0.1:0.5:1) were found for both samples (see Table 1). However, the line width of the two samples is different. The ^{29}Si MAS NMR signals of the PAH-containing sample exhibit a considerably larger line width (full width at half-maximum height, fwhm) than the *p*-GlcNAc-containing sample.

The line width of the ^{29}Si MAS NMR signals of amorphous silica is known to be determined by variations of the Si−O−Si bond angle.[52,53] This means that the Si−O−Si bond angle in PAH-containing silica, which is formed rapidly due to the accelerating influence of the electrostatic interactions (see above) exhibits a large variation, i.e., "structural disorder". In contrast, the slowly formed silica-*p*-GlcNAc nanocomposite shows a lower variation of the Si−O−Si bond angle. Nevertheless, the control sample exhibits the smallest line width, indicating that both organic additives influence the Si−O−Si bond angle (i.e., the local structure of the formed silica).

CONCLUSION

In summary, we can state that *p*-GlcNAc can be successfully silicified under biologically relevant conditions (i.e., at pH 5.5, using orthosilicic acid as the precursor compound). The prepared silica−*p*-GlcNAc nanocomposites exhibit a homogeneous *p*-GlcNAc dispersion. Solid-state ^{13}C NMR spectroscopy shows that the interaction between *p*-GlcNAc and silica obviously occur via hydrogen bonding, preferentially with the OH group located at carbon position C-6. However, this weak interaction does not result in an acceleration of the silica polycondensation process, in contrast to the behavior observed for positively charged polymers[54−60] such as PAH.

AUTHOR INFORMATION

Corresponding Author

*Phone: +49 351 463 37152. Fax: +49 351 463 37188. E-mail: eike.brunner@tu-dresden.de.

REFERENCES

(1) Kröger, N.; Deutzmann, R.; Sumper, M. *Science* **1999**, *286*, 1129–1132.

(2) Kröger, N.; Lorenz, S.; Brunner, E.; Sumper, M. *Science* **2002**, *298*, 584–586.
(3) Poulsen, N.; Kröger, N. *J. Biol. Chem.* **2004**, *279*, 42993–42999.
(4) Shimizu, K.; Cha, J.; Stucky, G. D.; Morse, D. E. *Proc. Natl. Acad. Sci. U.S.A.* **1998**, *95*, 6234–6238.
(5) Cha, J. N.; Shimizu, K.; Zhou, Y.; Christiansen, S. C.; Chmelka, B. F.; Stucky, G. D.; Morse, D. E. *Proc. Natl. Acad. Sci. U.S.A.* **1999**, *96*, 361–365.
(6) (a) Kröger, N.; Deutzmann, R.; Bergsdorf, C.; Sumper, M. *Proc. Natl. Acad. Sci. U.S.A.* **2000**, *97*, 14133–14138. (b) Sumper, M.; Brunner, E.; Lehmann, G. *FEBS Lett.* **2005**, *579*, 3765–3769. (c) Matsunaga, S.; Sakai, R.; Jimbo, M.; Kamiya, H. *ChemBioChem* **2007**, *8*, 1729–1735.
(7) Wenzl, S.; Hett, R.; Richthammer, P.; Sumper, M. *Angew. Chem., Int. Ed.* **2008**, *47*, 1729–1732. *Angew. Chem.* **2008**, *120*, 1753–1757.
(8) Brunner, E.; Richthammer, P.; Ehrlich, H.; Paasch, S.; Simon, P.; Ueberlein, S.; van Pée, K.-H. *Angew. Chem., Int. Ed.* **2009**, *48*, 9725–9727. *Angew. Chem.* **2009**, *121*, 9904–9907.
(9) Chiovitti, A.; Harper, R. E.; Willis, A.; Bacic, A.; Mulvaney, P.; Wetherbee, R. *J. Phycol.* **2005**, *41*, 1154–1161.
(10) Ehrlich, H. *Int. Geol. Rev.* **2010**, *52*, 661–699.
(11) Maeda, Y.; Jayakumar, R.; Nagahama, H.; Furuike, T.; Tamura, H. *Int. J. Biol. Macromol.* **2008**, *42*, 463–467.
(12) Nagahama, H.; Kashiki, T.; Nwe, N.; Jayakumar, R.; Furuike, T.; Tamura, H. *Carbohydr. Polym.* **2008**, *73*, 295–302.
(13) (a) Arias, J. L.; Fernández, M. S. *Chem. Rev.* **2008**, *108*, 4475–4482. (b) Weiss, I. M.; Schönitzer, V. *J. Struct. Biol.* **2006**, *153*, 264–277. (c) Ehrlich, H.; Maldonado, M.; Spindler, K. D.; Eckert, C.; Hanke, T.; Born, R.; Goebel, C.; Simon, P.; Heinemann, S.; Worch, H. *J. Exp. Zool. B* **2007**, *308*, 347–356.
(14) Brunner, E.; Ehrlich, H.; Schupp, P.; Hedrich, R.; Hunoldt, S.; Kammer, M.; Machill, S.; Paasch, S.; Bazhenov, V. V.; Kurek, D. V.; Arnold, T.; Brockmann, S.; Ruhnow, M.; Born, R. *J. Struct. Biol.* **2009**, *168*, 539–547.
(15) Ehrlich, H.; Simon, P.; Carrillo-Cabrera, W.; Bazhenov, V. V.; Botting, J. P.; Ilan, M.; Ereskovsky, A. V.; Muricy, G.; Worch, H.; Mensch, A.; Born, R.; Springer, A.; Kummer, K.; Vyalikh, D. V.; Molodtsov, S. L.; Kurek, D.; Kammer, M.; Paasch, S.; Brunner, E. *Chem. Mater.* **2010**, *22*, 1462–1471.
(16) Ehrlich, H.; Ilan, M.; Maldonado, M.; Muricy, G.; Bavestrello, G.; Kljajic, Z.; Carballo, J. L.; Shiaparelli, S.; Ereskovsky, A.; Schupp, P.; Born, R.; Worch, H.; Bazhenov, V. V.; Kurek, D.; Varlamov, V.; Vyalikh, D.; Kummer, K.; Sivkov, V. V.; Molodtsov, S. L.; Meissner, H.; Richter, G.; Steck, E.; Richter, W.; Hunoldt, S.; Kammer, M.; Paasch, S.; Krasokhin, V.; Patzke, G.; Brunner, E. *Int. J. Biol. Macromol.* **2010**, *47*, 132–140.
(17) Ehrlich, H.; Krautter, M.; Hanke, T.; Simon, P.; Knieb, C.; Heinemann, S.; Worch, H. *J. Exp. Zool. (Mol. Dev. Evol.)* **2007**, *308B*, 473–483.
(18) (a) McLachlan, J.; McInnes, A. G.; Falk, M. *Can. J. Botany* **1965**, *43*, 707–713. (b) Falk, M.; Smith, D. G.; McLachlan, J.; McInnes, A. G. *Can. J. Chem.* **1966**, *44*, 2269–2281. (c) Blackwell, J.; Parker, K. D.; Rudall, K. M. *J. Mol. Biol.* **1967**, *28*, 383–385. (d) Herth, W.; Barthlott, W. *J. Ultrastruct. Res.* **1979**, *68*, 6–15.
(19) Nassif, N.; Livage, J. *Chem. Soc. Rev.* **2011**, *40*, 849–859.
(20) Ogasawara, W.; Shenton, W.; Davis, S. A.; Mann, S. *Chem. Mater.* **2000**, *12*, 2835–2837.
(21) Jayakumar, R.; Nwe, N.; Tokura, S.; Tamura, H. *Int. J. Biol. Macromol.* **2007**, *40*, 175–181.
(22) Jayakumar, R.; Reis, R. L.; Mano, J. F. *e-Polymer* **2006**, *035*, 1–16.
(23) Madhumati, K.; Sudeesh Jumar, P. T.; Kavya, K. C.; Furuike, T.; Tamura, H.; Nair, S. V.; Jayakumar, R. *Int. J. Biol. Macromol.* **2009**, *45*, 289–292.
(24) Demadis, K. D.; Pachis, K.; Ketseti, A.; Stathoulopoulou, A. *Adv. Colloid Interface Sci.* **2009**, *151*, 33–38.
(25) Alonso, B.; Belamie, E. *Angew. Chem., Int. Ed.* **2010**, *49*, 8201–8204. *Angew. Chem.* **2010**, *122*, 8377–8380.
(26) Currie, H. A.; Perry, C. C. *Ann. Bot. (Oxford, U.K.)* **2007**, *100*, 1383–1389.
(27) Kröger, N. *Curr. Opin. Chem. Biol.* **2007**, *11*, 662–669.
(28) Brunner, E.; Gröger, C.; Lutz, K.; Richthammer, P.; Spinde, K.; Sumper, M. *Appl. Microbiol. Biotechnol.* **2009**, *84*, 607–616.
(29) Vournakis, J. N.; Demcheva, M.; Whitson, A.; Gurica, R.; Pariser, E. R. *J. Trauma* **2004**, S3–S6.
(30) Vournakis, J. N.; Finkeilsztein, S.; Pariser, E. R.; Helton, M. PCT Int. Appl., WO 9515343, A1 19950608, 1995.
(31) Vrieling, E. G.; Gieskes, W. W. C.; Beelen, T. P. M. *J. Phycol.* **1999**, *35*, 548–559.
(32) Coradin, T.; Eglin, D.; Livage, J. *Spectroscopy* **2004**, *18*, 567–576.
(33) Tanner, S. F.; Chanzy, H.; Vincendon, M.; Roux, J. C.; Gaill, F. *Macromolecules* **1990**, *23*, 3576–3583.
(34) Pines, A.; Gibby, M. G.; Waugh, J. S. *J. Chem. Phys.* **1973**, *59*, 569–590.
(35) Metz, G.; Wu, X.; Smith, S. O. *J. Magn. Reson. A* **1994**, *110*, 219–227.
(36) Fung, B. M.; Khitrin, A. K.; Ermolaev, K. *J. Magn. Reson.* **2000**, *142*, 97–101.
(37) Ferguson, D. B.; Haw, J. F. *Anal. Chem.* **1995**, *67*, 3342–3348.
(38) Brauer, G. *Das Handbuch der Präperativen Anorganischen Chemie*; Enke Verlag: Stuttgart, Germany, 1975.
(39) Rinaudo, M. *Prog. Polym. Sci.* **2006**, *31*, 603–632.
(40) Cárdenas, G.; Cabrera, G.; Taboada, E.; Miranda, S. P. *J. Appl. Polym. Sci.* **2004**, *93*, 1876–1885.
(41) Kameda, T.; Miyazawa, M.; Ono, H.; Yoshida, M. *Macromol. Biosci.* **2005**, *5*, 103–106.
(42) Kono, H. *Biopolymers* **2004**, *75*, 255–263.
(43) Noishiki, Y.; Takami, H.; Nishiyama, Y.; Wada, M.; Okada, S.; Kuga, S. *Biomacromolecules* **2003**, *4*, 896–899.
(44) Hsiao, C. N.; Huang, K. S. *J. Appl. Polym. Sci.* **2005**, *96*, 1936–1942.
(45) Tilburey, G. E.; Patwardhan, S. V.; Huang, J.; Kaplan, D. L.; Perry, C. C. *J. Phys. Chem. B* **2007**, *111*, 4630–4638.
(46) Ehrlich, H.; Deutzmann, R.; Brunner, E.; Cappellini, E.; Koon, H.; Solazzo, C.; Yang, Y.; Ashford, D.; Thomas-Oates, J.; Lubeck, M.; Baessmann, C.; Langrock, T.; Hoffmann, R.; Wörheide, G.; Reitner, J.; Simon, P.; Tsurkan, M.; Ereskovsky, A. V.; Bazhenov, V. V.; Hunoldt, S.; Mertig, M.; Vyalikh, D. V.; Molodtsov, S. L.; Kummer, K.; Worch, K.; Smetacek, V.; Collins, M. J. *Nature Chem.* **2010**, *2*, 1084–1088.
(47) Iler, R. K. *The Chemistry of Silica*; Wiley−Interscience: New York, 1979.
(48) Brunner, E.; Lutz, K.; Sumper, M. *Phys. Chem. Chem. Phys.* **2004**, *6*, 854–857.
(49) Coradin, T.; Livage, J. *Colloids Surf. B* **2001**, *21*, 329–336.
(50) Mizutani, T.; Nagase, H.; Fujiwara, N.; Ogoshi, H. *Bull. Chem. Soc. Jpn.* **1998**, *71*, 2017–2022.
(51) Massiot, D.; Fayon, F.; Capron, M.; King, I.; Le Calvé, S.; Alonso, B.; Durand, J. O.; Bujoli, B.; Gan, Z.; Hoatson, G. *Magn. Reson. Chem.* **2002**, *40*, 70–76.
(52) Thomas, J. M.; Klinkowski, J.; Ramdas, S.; Hunter, B. K.; Tennakoon, D. T. B. *Chem. Phys. Lett.* **1983**, *102*, 158–162.
(53) Radeglia, R.; Engelhardt, G. *Chem. Phys. Lett.* **1985**, *114*, 28–30.
(54) Helmecke, O.; Hirsch, A.; Behrens, P.; Menzel, H. *J. Colloid Interface Sci.* **2008**, *321*, 44–51.
(55) Menzel, H.; Horstmann, S.; Behrens, P.; Bärnreuther, P.; Krueger, I.; Jahns, M. *Chem. Commun.* **2003**, 2994–2995.
(56) Behrens, P.; Baeuerlein, E. *Handbook of Biomineralisation−Biomimetic and Bioinspired Chemistry*; Wiley−VCH: Weinheim, Germany 2007.
(57) Patwardhan, S. V.; Clarson, S. J. *Silicon Chem.* **2002**, *1*, 207–214.
(58) Patwardhan, S. V.; Mukherjee, N.; Clarson, S. J. *Silicon Chem.* **2002**, *1*, 47–57.
(59) Patwardhan, S. V.; Clarson, S. J. *Mater. Sci. Eng., C* **2003**, *23*, 495–499.
(60) Belton, D. J.; Patwardhan, S. V.; Annenkov, V. V.; Danilovtseva, E. N.; Perry, C. C. *Proc. Natl. Acad. Sci. U.S.A.* **2008**, *105*, 5963–5968.